Microstructure of thermally grown and deposited alumina films probed with positrons

Bertram Somieski,* Lester D. Hulett, and Jun Xu

Oak Ridge National Laboratory, Chemical & Analytical Sciences Division, Oak Ridge, Tennessee 37831

Bruce A. Pint and Peter F. Tortorelli

Oak Ridge National Laboratory, Metals & Ceramics Division, Oak Ridge, Tennessee 37831

Bent Nielsen and Palakkal Asoka-Kumar

Brookhaven National Laboratory, Department of Physics, Upton, New York 11973

Ryoichi Suzuki and Toshiyuki Ohdaira

Electrotechnical Laboratory, Quantum Radiation Division, Tsukuba, Ibaraki 305, Japan

Aluminum oxide films used for corrosion protection of iron and nickel aluminides were generated by substrate oxidation as well as plasma and physical vapor depositions. The films grown by oxidation were crystalline. The others were amorphous. Defect structures of the films were studied by positron spectroscopy techniques. Lifetimes of the positrons, and Doppler broadening of the γ photons generated by their annihilation, were measured as functions of the energies with which they were injected. In this manner, densities and sizes of the defects were determined as functions of depths from the outer surfaces of the films. Alumina films generated by oxidation had high densities of open volume defects, mainly consisting of a few aggregated vacancies. In the outer regions of the films the structures of the defects did not depend on substrate compositions. Positron lifetime measurements, and the S and W parameters extracted from Doppler broadening spectra, showed uniform distributions of defects in the crystalline Al_2O_3 films grown on nickel aluminide substrates, but these data indicated intermediate layers of higher defect contents at the film/substrate interfaces of oxides grown on iron aluminide substrates. Amorphous films generated by plasma and physical vapor deposition had much larger open volume defects, which caused the average lifetimes of the injected positrons to be significantly longer. The plasma deposited film exhibited a high density of large cavities. [S0163-1829(99)09409-6]

I. INTRODUCTION

Materials that can withstand high temperatures without losing their mechanical properties have many practical applications. Transition-metal aluminides, e.g., those of iron and nickel, are particularly interesting because of their good high-temperature corrosion resistance and other attractive properties.[1]

Oxide coatings are effective for protecting metals and alloys from chemical reaction with environmental gases. Many different techniques for producing them have been studied. For oxidation resistant alloys, an external oxide layer forms during oxidation of the substrate, which occurs in the course of its use in most environments. For the alloys in this study, alumina films were formed by both oxidation and vapor deposition. Trace elements in the substrates, such as Hf, Y, or Zr, are beneficial to the growth or the films, primarily by improving their adhesion to the substrate, cf. Pint.[2]

Defect structures of the films are important factors in the diffusion processes involved in their growth kinetics, and may affect the mechanical properties of the films.[3] Therefore, positron spectroscopy could serve as a valuable characterization tool for such surface oxides.

Positron spectroscopy is a useful method for investigating numerous kinds of open volume defects, such as mono- and divacancies, vacancy clusters, or dislocations, in metals, e.g., Schaefer,[4] semiconductors, e.g., Hautojärvi,[5] and even in ionic crystals, e.g., Hyodo.[6] With positron lifetime spectroscopy it is possible to obtain information on the type and the density of the respective defects simultaneously. Doppler broadening measurements of positron annihilation processes provide rapid measurements of defect concentrations. Positron spectroscopy data are not distorted by internal stress, interstitials, or pure antisite defects. Unambiguous information about open volume defects is thus provided.

II. EXPERIMENTS AND ANALYSIS

A. Samples

The protective aluminum oxide films on the specimens studied in this work were on the order of $1\,\mu$m in thickness. In order to perform measurements on such specimens it is necessary to use monoenergetic (''slow'') beams of positrons. Fast positrons from ordinary radioisotope sources have energies that are so high ($E_{kin} > 500$ keV), and of such a large spread as to make them unusable. Positrons from such sources penetrate the substrates and generate backgrounds that obscure the information from the films. The beams of slow positrons used in this work had energies that were defined to within 100 eV or less, thus allowing control of the depths to which the oxide films were penetrated. Measurements of both the Doppler broadening of the energies of the γ photons resulting from the annihilating positrons (DBAR)

TABLE I. Sample specifications and preparations; experiments.

Sample	Substrate	Procedure of producing the layer	Layer structure	Layer thickness	DBAR	beam lifetime measurements
NAHf	$Ni_{49}Al_{51}Hf_{0.05}$	Substrate oxidation		0.4 μm [a]	●	●
NATZ	$Ni_{49.3}Al_{50.4}Ti_{0.21}Zr_{0.08}$	in flowing O_2	α-Al_2O_3	0.8 μm [a]	●	
FAY1	$Fe_{69.9}Al_{28}Cr_2Y_{0.1}$	@ 1200 °C for 2 h		1 μm [a]	●	●
FAY3	$Fe_{69.7}Al_{28}Cr_2Y_{0.3}$			1 μm [a]	●	
NA	$Ni_{49.8}Al_{50.2}$	Al^+ - plasma deposition	amorphous	1 μm [b]	●	●
FAZr	$Fe_{66.9}Al_{28}Cr_5Zr_{0.1}$	Physical vapor depos.	Al_2O_3	5 μm [c]	●	●

[a]Values are obtained from SEM and TEM micrographs (Refs. 7,8).
[b]See Brown *et al.* Ref. 9 or Monteiro *et al.* (Ref. 10,11).
[c]See Barbee (Ref. 12).

and of the lifetimes of the positrons after injection were made. Table I contains a description of the samples examined.

Al_2O_3 films on transition-metal aluminides were investigated with variable energy positron Doppler-broadening measurements and with variable energy positron lifetime spectroscopy. The nickel aluminides and FAZr were cast, resulting in a grain size $d_g > 100$ μm, whereas the samples FAY1 and FAY3 were made by powder metallurgy, $d_g \approx 1$ μm.[8,7] All samples were polished with 0.3 μm alumina prior to oxidation or coating deposition. FAY1 and FAY3 were chosen because they form interfacial (metal-alumina) voids of 50–150 nm diameter upon oxidation, see, for example Pint *et al.*[7,13] Samples of NAHf and NATZ do not show voids after oxidation for 2 h at 1200 °C.[14]

B. DBAR measurements

The Doppler-broadening experiments on the samples NATZ, FAY3, NA, and FAZr, cf. Table I, were carried out with the slow-positron beam at *Brookhaven National Laboratory*. Details and specifications are described in the paper of Lynn and Lutz.[15] The run for the samples NAHf and FAY1, cf. Table I, was done with the slow-positron beam in the *Positron Laboratory* at the *University Halle, Germany.*

C. Variable energy positron lifetime measurements

The pulsed slow-positron beam at the *Electrotechnical Laboratory, Tsukuba* was used for the variable energy positron lifetime measurements. Details of the apparatus are described by Suzuki *et al.*[16] Approximately $0.5–0.7 \times 10^6$ single events were collected for each single spectrum. The spectrometer had a resolution of 300–315 ps full width at half maximum (FWHM). As already described in a preliminary paper,[17] a small portion of positrons were reflected from the sample or the sample holder generating a very long lifetime component. These lifetime components were discarded in the analysis. We are sure that this component did not originate from positronium states, as it sometimes did not appear at very low positron energies, when positronium formation has highest probability, cf. $E_{e+} = 0.5$ keV in Fig. 9, but sometimes appeared when all positrons are assumed to be implanted into the metallic substrate, cf. $E_{e+} = 23$ keV in Fig. 9 and discussion in Secs. III and III B 2.

In a few of the spectra, satellite peaks appeared after the main peak. Then, only earlier parts of the spectra were considered and a flat part of the spectrum with scattering only was used to determine the background.

D. Standard positron lifetime measurements

Material of the compositions $Fe_{69.9}Al_{28}Cr_2Y_{0.1}$, $Ni_{49.8}Al_{50.2}$, and $Ni_{49}Al_{51}Hf_{0.05}$, the raw substrate materials for samples FAY1, NA, and NAHf, respectively, were analyzed by standard positron lifetime spectroscopy. A fast-fast coincidence positron lifetime spectrometer with Pilot-U scintillators having a resolution function of 220 ps FWHM was used. The source material was 14 μCi ^{22}NaCl deposited on a 2 μm Al foil. About 4.5×10^6 single events were collected for these spectra. Source correction was made as described elsewhere.[18]

E. Numerical analysis

A small portion of the positrons injected into solids annihilate with core electrons of the atoms in that material. Core electrons have high momentum, causing Doppler broadening of the photons emitted. If open-volume defects are present in the solid, a large percentage of the positrons will be trapped in regions where core electron density is low, leaving only the low-energy valence electrons for annihilation. As a result, the Doppler broadening will be lower. Defect trapping will cause the S parameter to increase, cf. Sec. II F.

The S parameter curves were analyzed by means of the program VEPFIT.[19,20] A Makhov profile,[21,22]

$$P(z,E) = \left(\frac{m}{z_0}\right)\left(\frac{z}{z_0}\right)^{m-1} \exp\left[-\left(\frac{z}{z_0}\right)^m\right], \quad (1)$$

z is the implantation depth, E is the positron energy, was used to describe the positron implantation. Here the abbreviations

$$z_0 = 1.13 z_m; \quad z_m = (A/\rho)E^n \quad (2)$$

apply, where ρ is the physical density of the material and z_m is the mean implantation depth for the given energy; m, n, and A are empirical constants. We choose $m = 2$, $A = 4 \mu$g/(cm^2 keV^n), and $n = 1.62$ according to the results of Vehanen *et al.*[23] We assumed the mass density of the α-Al_2O_3 layers, cf. Table I, to be not markedly different

from the theoretical value of $\rho = 3.97$ g/cm^3 as the micrographs of these and all similar films did not show a large volume fraction of voids.[13] For the plasma deposited amorphous alumina layer on NA, cf. Table I, we started with the same value as for the α-Al$_2$O$_3$, but we also tried smaller values. For more details see Sec. III C 1.

All lifetime spectra were analyzed by means of the program LIFESPECFIT written by Puska.[24] Single lifetime spectra were recorded for all experiments at very low positron energies, $E_{e^+} \lesssim 1$ keV approximately, dependent on the sample. We interpret this effect to be due to the trapping of the positrons in surface states, in particular as these components were also found with decreasing intensity at slightly higher positron energies together with components originating from the film. At those higher energies some of the positrons diffuse back to the surface, whereas the other ones are trapped inside the film. For this reason the surface lifetime components were fixed until disappearance to the values for shallow deposition.

The width of the resolution function of the beam-lifetime spectra was fitted within a certain range of 300–315 ps, approximately, because it was not to be expected that the resolution function of the spectra is independent of the positron implantation energy.

F. S vs W plots

The annihilation process of positrons by electrons requires that both energy and momentum be conserved. Because of the conversion of the masses of the electron and positron into photons, small changes in the momenta of the electrons cause large shifts of energy from one photon to the other, leading to a high degree of Doppler broadening of the 511 keV annihilation peaks. The S parameter and the W parameter are empirical measures of the degree of broadening. The S parameter is defined as the ratio of the area of the mid portion of the annihilation peak to the area of the entire peak. The W parameter is the ratio of the area of the wings of the peak to its entire area. The width of the regions for both parameters is user chosen, frequently so that the defect-free material has $S = 0.5$ and $W = 0.05$. S parameters are larger when positrons annihilate mostly with low-momentum electrons. W parameters are larger, and S parameters are smaller, when annihilation occurs with core electrons of atoms, cf. West.[25] For atoms of transition metals such as iron and nickel, appreciable amounts of annihilation occur with the outer core electrons, $3d$ electrons, causing increases in the W parameters.

In the analysis of films by Doppler broadening measurement of the annihilation peaks, it is quite useful to plot the S parameters vs the W parameters, see the article of Clement et al.[26] for example. Figure 1 is a three-dimensional illustration of the relationship between the S and W parameters and positron injection energies. For Figs. 2, 3, 6, 7, 11, and 14 the S-W diagrams are shown as two-dimensional plots, accompanying the plots of S parameters vs positron injection energies.

For monolithic materials, whose compositions and defect structures do not vary with depth from their surfaces, the S vs W diagrams consist of clusters of points, for which all the S and W parameters are approximately the same. An example
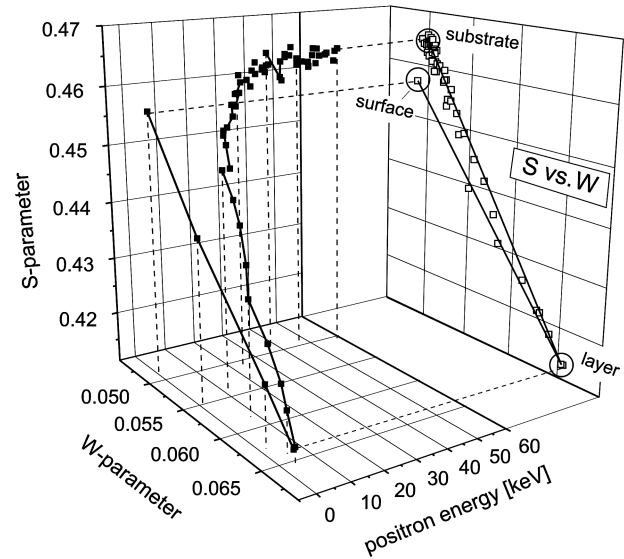
FIG. 1. Three-dimensional plot of S and W parameter in sample NATZ as a function of positron energy and derived S vs W plot.

of this is discussed in Sec. III D. For layered films of different structure, in which the positrons penetrate more than one layer, the S and W parameters vary with positron injection energy according to different schedules, and their diagrams are extended from clusters of points to line segments. The first point in Fig. 1, having the parameter triple $(E[\text{keV}], W, S) = (0.463, 0.0487, 0.4568)$, indicates the (positron annihilation) properties of the surface, the two points obtained at positron energies of 3 and 4 keV, $(3.001, 0.0655, 0.4136)$ and $(4.003, 0.0653, 0.4136)$, represent the properties of the Al$_2$O$_3$ layer. Higher positron injection energy distributes the positrons between the oxide layer and the metal substrate, extending the data points to a line. Finally all positrons annihilate in the substrate, indicated by the cluster of points around $(W, S) = (0.049\,9, 0.469\,38)$.
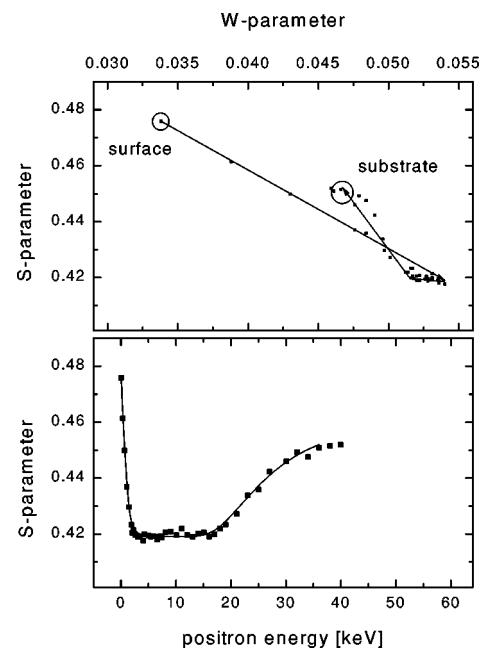
FIG. 2. S parameter in sample FAY1 as a function of positron energy and S vs W plot.
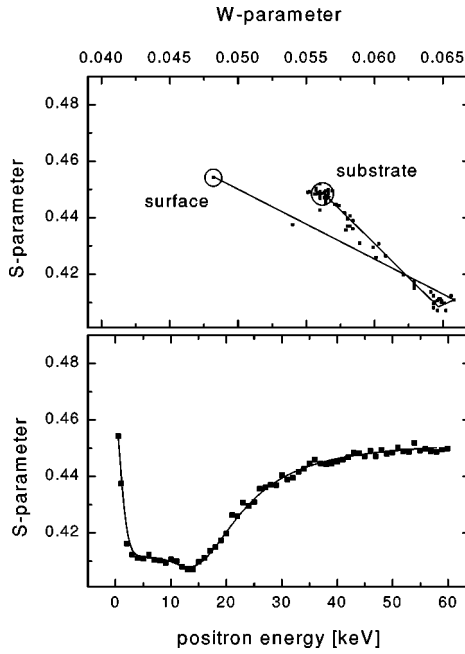
FIG. 3. S parameter in sample FAY3 as a function of positron energy and S vs W plot.

In general, by extending the appearing line segments to their intersecting points, one can obtain from those apices the S and W parameters of each layer, see for example Clement *et al.*[27,26]

III. RESULTS AND DISCUSSION

The apparent formation of positronium in Al_2O_3 has been demonstrated after special treatments of Al_2O_3, like neutron irradiation and annealing, cf. Hasegawa *et al.*[28] or Nagashima *et al.*,[29] or anodic deposition, cf. van Hoecke *et al.*,[30] or in fine grained powders, cf. Dauwe and Mbungu-Tsumbu[31] as well as after calcination, cf. Ewertowski *et al.*,[32] or sintering of powders, cf. Brauer *et al.*[33] In contradiction to those results we found no indication of free positronium inside our samples, neither by Doppler broadening of annihilation radiation (DBAR) measurements[34] nor by the variable energy positron lifetime spectroscopy, cf. Sec. II C. Even though SEM micrographs showed some large cavities of up to 100 nm diameter,[13] their volume fraction seems not to be sufficient to achieve the threshold for a positronium component in the spectrum.

For convenient comparison, the figures containing DBAR measurements, Figs. 2, 3, 6, 7, 11, and 14 and the figures containing positron lifetime analysis, Figs. 8, 9, 12, and 13, are equally scaled. The lines in the plots S parameter vs energy are fits by means of VEPFIT; the lines in the S vs W plots and in the lifetime parameter plots are to guide the eye.

A. Unoxidized substrates

1. Fe_3Al Substrate

There are few papers about analyzing the defect structure of Fe_3Al alloys by means of positron annihilation spectroscopy. For example, Jirásková *et al.* found in cast and annealed ingots of $Fe_{72}Al_{28}$ a defect lifetime of 185 ps,[35] which

they attributed to positron annihilation in single vacancies. From that result the bulk lifetime in defect free material was calculated to be 118 ps. In as-cast material of slightly different composition ($Fe_{76.3}Al_{23.7}$), Schaefer *et al.* measured a single-component positron lifetime spectrum of 112 ps, indicating that the vacancies concentration was below the threshold for positron lifetime spectroscopy.[36] This is consistent with the conclusions of Wang *et al.*[37] and Dlubek *et al.*[38] that increasing percentage of aluminum increases the density of remaining vacancies, although Wang *et al.* still found excess vacancies after furnace cooling of $Fe_{78}Al_{22}$. If one assumes their spectrum ($\tau_1 = 113$ ps, $\tau_2 = 223$ ps, $I_1 = 78\%$, $I_2 = 22\%$) to consist of defect lifetime and reduced bulk lifetime, so that the two-state trapping model may apply, cf. Bergerson and Stott,[39] or Seeger,[40] the bulk lifetime τ_b of the defect-free material

$$\frac{1}{\tau_b} = \frac{I_0}{\tau_1} + \frac{I_2}{\tau_2} \tag{3}$$

is calculated to be 127 ps, which is much higher than the value given by Schaefer *et al.* or Jirásková *et al.* In addition, Wang *et al.* found in $Fe_{78}Al_{22}$ only a neglectible second component besides the main lifetime of 123 ps that is also higher than the bulk lifetime value given by Jirásková *et al.*

We found, however, in the unoxidized substrate of sample FAY1 ($Fe_{69.9}Al_{28}Cr_2Y_{0.1}$) a two-component spectrum with the values: $\tau_1 = 165$ ps, $\tau_2 = 291$ ps, $I_1 = 73.5(\pm 0.8)\%$, $I_2 = 26.5(\pm 0.8)\%$. We believe that the second component originates from grain boundaries, which is reasonable due to its lifetime value and the high volume density of grain boundaries in this material, cf. Sec. II A. If we assume that in the present material the positron diffusion constant D_+ has, similar to other materials, a value of the order of 1 cm^2/s, and the bulk positron lifetime to be close to the value given by Schaefer *et al.*, we can adopt the results of Hübner *et al.*,[41] who calculated in copper ($D_+ = 1.5$ cm^2/s, $\tau_b = 110$ ps) the fraction of positrons reaching the grain boundaries as a function of grain size and trapping rate. We obtain from there, that the trapping rate should have values $\kappa = 2-4 \times 10^{10}$ s^{-1}, and, using the trapping coefficient given by Schaefer *et al.*, $\mu_{1v} = 4 \times 10^{14}$ s^{-1}, that the concentration of single vacancies, $c_{1v} = \kappa/\mu_{1v}$, in our material is of the order of 50–100 ppm.

2. NiAl substrate

It is well known that both stoichiometric and hypostoichiometric $Ni_{50}Al_{50}$ retain high densities of Ni vacancies after slow cooling.[42] In $Ni_{49.8}Al_{50.2}$ and in $Ni_{49}Al_{51}Hf_{0.05}$ we found saturated trapping in defect sites of a single kind. The positron lifetimes were (175 ± 1) ps and (172 ± 1) ps, respectively. We agree with the conclusions of Shimotomai *et al.*, Kim *et al.*, and Fu *et al.*[43–45] that all positrons are trapped in single vacancies in the Ni sublattices. Fu *et al.* have calculated that the formation enthalpy for aluminum vacancies is at least twice as high as that for vacancies in the nickel sublattice, giving further support to our view that positron trapping in aluminum vacancies is not likely.

Kim reports that in stoichiometric $Ni_{50}Al_{50}$ the vacancy density is above 0.1 at. %,[44] which is so high that all positrons are trapped. This result is consistent with the calcula-
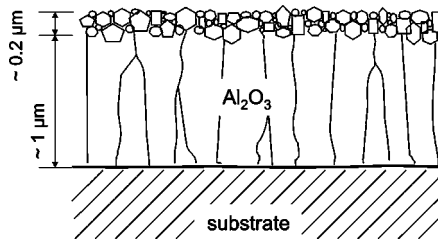
FIG. 4. Schematic structure of the Al_2O_3 layers grown by substrate oxidation as observed by electron microscopy, cf. Pint *et al.* (Refs. 8, 14, and 7).

tions of Fu *et al.*[45] Therefore, we have to assume that positrons are trapped in the Ni sublattice. That is in contradiction to the results of Schaefer *et al.* who found material of very low vacancy density (below the threshold) after annealing.[36]

Deng *et al.* report that annealing of $Ni_{50}Al_{50}$ at 1100 °C produces large voids which induce long lifetime components in the positron spectra.[46] These results could also be explained, however, on the basis of the specimens being cut and polished after the heat treatments. The large lifetime components could have been due to the effects of mechanical abrasion, as reported by Park *et al.* for pure iron[47] and by Somieski and Krause-Rehberg for steel.[48]

B. Layers grown by substrate oxidation

1. Doppler-broadening results

Figures 2 and 3 are plots of S parameters, extracted from measurements of the Doppler-broadened positron annihilation peaks, recorded as functions of the energies with which positrons were injected in the surface films of the FAY1 and FAY3 samples. The similarity in the shapes of the two curves is to be expected, because the compositions of the substrates were nearly the same, and the oxidation conditions under which the films were grown were identical, cf. Table I. The S parameters recorded for small positron injection energies, ranging from 250 eV to 2 keV approximately, are influenced by annihilation of positrons trapped in surface states. For injection energies greater than this range, the positrons penetrate sufficiently far beyond the surface as not to be able to diffuse back. S parameters measured for these energies represent annihilation events taking place at sites inside the oxide film. The rapid decrease of S parameters at energies of 250 eV–2 keV was also observed by Vehanen *et al.*[23]

S vs W diagrams accompany the respective S parameter plots of Figs. 2 and 3. Each diagram consists of three extended curves, which indicates that the oxide films are composed of two layers, as the two lines, indicating the change in the positron distribution from surface or substrate to the layer, do not join in one point as it is expected for a uniform layer, see for example Figs. 6 and 11. SEM micrographs of cross sections of the two films also suggest two layers, cf. Ref. 8: The interior part of the film, closest to the substrate, has ≈ 1 μm long, columnar grains, while the outer surface regions of the film has smaller, equiaxed grains, see Fig. 4. The obvious two-layer nature of the FAY1 film, as indicated by the S-W diagram, was not apparent in the S parameter vs energy curve. The VEPFIT program that is used to interpret S

vs energy plots is sometimes applicable to multilayered surface structures, but we do not think it is applicable to the FAY1 data, as the data fit a smooth curve quite well.

The S-W diagram for the FAY3 film also suggests a two layer structure. The existence of a second layer is not as clearly seen as for the FAY1 film. The S vs energy plot for the FAY3, however, does certainly suggest a two-layer structure, since after the straight part from 3 to 9 keV the S parameter decreases again and forms a dip. Therefore, the VEPFIT program was used to fit a curve to the experimental points, assuming the existence of two layers.

The very steep drop of the S parameter, for the positron injection energy range of 0.25–2 keV, indicates a high density of trapping centers in the outer surface layer that reduces the positron diffusion length. If one uses the formula

$$L_+ = 105 \ \text{Å} \left[E_0 / (1 \ \text{keV}) \right]^{1.6}, \tag{4}$$

obtained from Saarinen *et al.*[49] and adjusted for the density of the Al_2O_3, where E_0 is the half-width of the change in the $S(E)$ curve, to calculate the effective positron diffusion length in the Al_2O_3 layer $L_+^{(l)}$, the results $^{(FAY1)}L_+^{(l)} = 17$ nm and $^{(FAY3)}L_+^{(l)} = 16$ nm are in good agreement with the fitted L_+ of VEPFIT, cf. Table III in Sec. IV. We believe therefore, that the fit done by VEPFIT is not somehow perturbed.

The substrates in FAY1 and FAY3 differ only slightly in their content of yttrium, and the conditions under which the films are formed were identical in both cases, cf. Table I. We, hence, assume both samples to be very similar *a priori*. To our knowledge the higher amount of yttrium in the sample FAY3 should only influence the outer part of the Al_2O_3 layer. Yttrium is known to segregate to alumina grain boundaries where it inhibits grain growth.[50] Thus, a higher Y content may result in more segregation and thus a finer outer-layer grain size.

Figure 2 shows that for the FAY1 sample the S parameter curve is flat over the positron injection energy range of 2.5–15 keV. But for the FAY3 specimen, Fig. 3 shows a significant decrease in the S parameter starting at 8 keV positron implantation energy, approximately. We ascribe the decrease for the FAY3 sample, to the combination of the increased amount of yttrium in the substrate, which segregates at the grain boundaries of the Al_2O_3 film,[2,14] and the increased positron diffusion lengths together with the perhaps slightly smaller grain size for the interior of the α-Al_2O_3 film in specimen FAY3, cf. Fig. 15. We conclude that, therefore, the positrons injected into the interior of this films have higher probabilities of reaching the grain boundaries and annihilating with electrons of yttrium atoms than those positrons injected at lower energies. The annihilation with the outer $4d$ electrons of the yttrium atoms should broaden the 511 keV peak, since those electrons have higher momentum. The S parameter measurements on FAY1 and FAY3 were not made with the same facility, cf. Sec. II B. A simple comparison of the absolute magnitudes of the S parameters can therefore not be drawn. On the condition that both samples are *a priori* similar, as mentioned above, it is possible, however, to normalize the two sets of data. A simple linear normalization formula was used:

$$S' = kS + S_0. \tag{5}$$
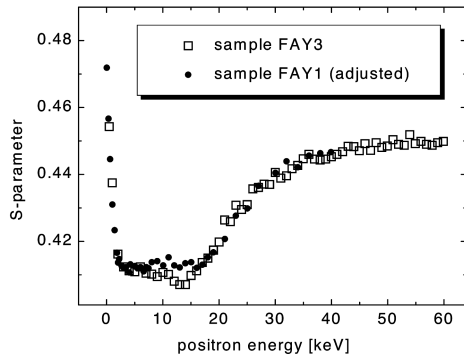
FIG. 5. Comparison of the *S* parameters of samples FAY1 and FAY3 adjusted using formula (5).

Using coefficient values of $k=1.0512$ and $S_0=-0.0284$, the *S* parameters of the FAY1 specimen were transformed in a manner that its S' values were almost identical for the 0.25–5 keV and 20–40 keV energy ranges, compared with FAY3, cf. Fig. 5. These ranges cover surface, outer layer part, and substrate region. This result vindicates our assumption, explained above, that the only difference between samples FAY1 and FAY3 is in the yttrium content, and that this changed the *S* parameters only for the interior part of the α-Al_2O_3 layer (energy range of 8–15 keV). As expected, the transforming of the data did not change the values of the diffusion length or layer thickness in the VEPFIT fit.

The *S* parameter curve and the *S* vs *W* plot for the NATZ specimen indicate that the Al_2O_3 film is uniform in its structure and thinner, see Fig. 6, than those on the iron aluminide substrates. It can be seen from the *S* parameter curves in Figs. 3 and 6 that for positron injection energies $E_{e^+} \leq 4$ keV, the *S* parameters of the Al_2O_3 film on the NATZ specimen are almost identical to those of the FAY3 film, suggesting that positron diffusion lengths are about the same
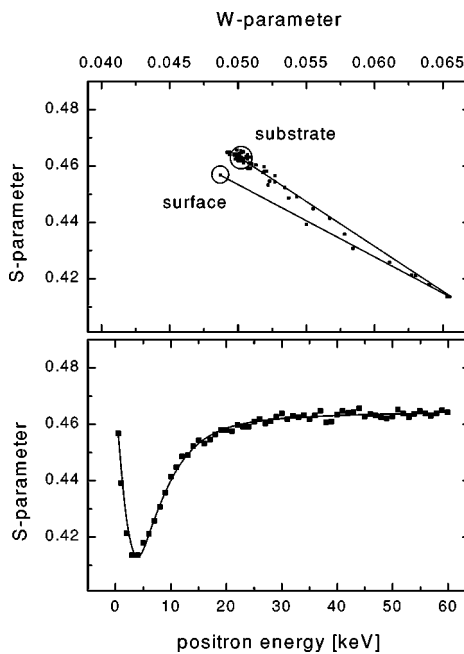
FIG. 6. *S* parameter in sample NATZ as a function of positron energy and *S* vs *W* plot.
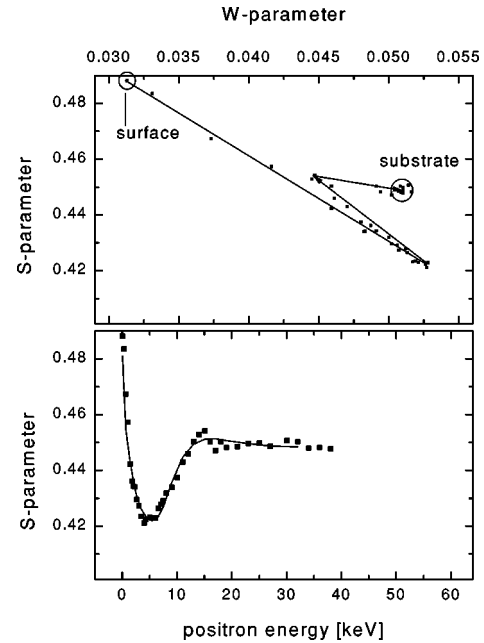
FIG. 7. *S* parameter in sample NAHf as a function of positron energy and *S* vs *W* plot.

for both films. VEPFIT actually gave almost the same diffusion lengths, cf. Table III in Sec. IV. Combined with the identity of the vertices, indicating surface and layer properties in the *S* vs *W* plots in Figs. 3 and 6, the defect structure and defect density of both films appear to be very similar. In future work, films of thickness comparable to those on iron aluminide substrates will be grown on nickel aluminide substrates and will be examined by positron spectroscopy to determine if the structures remain similar.

The *S* parameter curve for the NATZ sample was measured at the *Brookhaven National Laboratory*, and that for the NAHf sample, see Fig. 7, was recorded at the *University Halle, Germany*. As for the sample FAY1 we transformed the *S* values of sample NAHf with formula (5) and the above given constants. The resulting S'-parameter value for the film was essentially the same as for the NATZ. The *S* parameters for the outer surface regions of the two films did not agree, however. A rather large difference between both samples was found in the *S* parameter of the oxidized substrates: $^{(NATZ)}S^{(s)}=0.4635$, $^{(NAHf)}S'^{(s)}=0.4456$. The *S* parameters of the Al_2O_3 films grown on the iron aluminide substrates are also in this range, see Fig. 15. We conclude, therefore, that the influence of the substrate upon the positron-detectable properties of the Al_2O_3 layers (in case of the structured oxide layers on the iron aluminide substrates the outer part of the layer), is rather small.

The thickness of the film on the NAHf has been calculated by VEPFIT to be about $d_l=345$ nm, in reasonable agreement with the micrograph measurements of $d_l \approx 400$ nm.[51] Taking into account the VEPFIT-calculated thickness of the alumina films on the iron aluminide substrates of 1.5–1.8 μm, cf. Fig. 15, the oxide growth on the iron aluminide substrate substantially higher then on the nickel aluminide substrate.

For energies ranging between 4–5 keV, a slight increase in the *S* parameters was measured in sample NAHf. Positron diffusion length in the oxide layer is $^{(NAHf)}L_+^{(l)} \approx 24$ nm. Be-
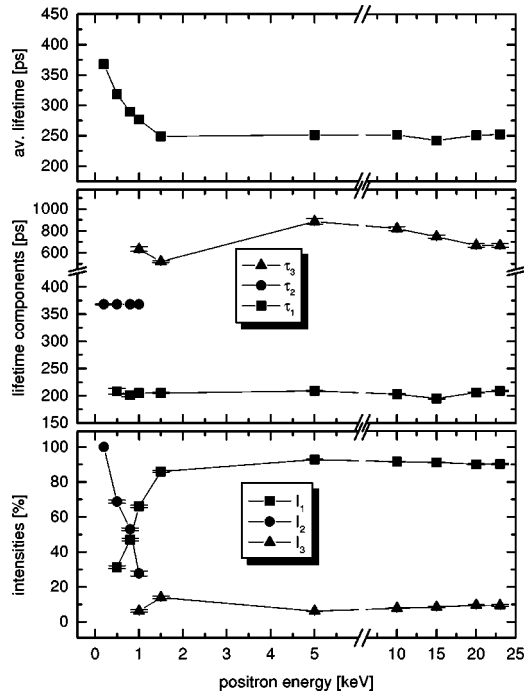
FIG. 8. Positron lifetime parameters as a function of positron energy in sample FAY1, cf. Table I. Error bars have been omitted since the errors are smaller than the symbol size; lines are to guide the eye.

FIG. 9. Positron lifetime parameters as a function of positron injection energy in sample NAHf, cf. Table I. If no explicit error bars are shown, they are smaller than the symbol size; lines are to guide the eye.

cause the portion of positrons implanted in regions $z > d_l - L_+^{(l)}$ is smaller than 1.5% for $E_{e^+} = 5$ keV, we think that this increase is due primarily to changes in the oxide layer, rather than to effects of the interface or substrate.

In contradiction to sample NATZ, where the α-Al_2O_3 film was found to be uniform in its structure, the small peak in the NAHf S-parameter curve around 15 keV indicates a more complicated film structure. This is strongly supported by the S vs W plot in Fig. 7. We ascribe this effect to preferred trapping at the metal-oxide interface. To make a proper fit we assumed the interface region to be rather small, $d_i \approx 5$ nm, and to have complete trapping, $L_+^{(i)} \rightarrow 0$. This result is in contradiction to the results from the S-parameter curves of the other three oxidized samples FAY1, FAY3, and NATZ, in which we did not find any indication of preferred trapping at an interface region of markedly different properties. In addition, the peak in the S parameter at 15 keV is not reflected in the lifetime measurements, cf. Fig. 9.

The greater thickness of the oxide films on the iron aluminide substrates, cf. Table I, prevented accurate estimates of positron diffusion lengths in them. Using the VEPFIT program, curves were fitted to the S-parameter curves, assuming a wide range $L_+^{(s)} = 5$–200 nm, of diffusion lengths. The quality of the fit to the experimental data was not sensitive to the choice of the diffusion length.

2. Results of variable energy positron lifetime spectroscopy

Figures 8 and 9 show plots of the average and the mean positron lifetimes as well as their respective intensities, obtained from deconvolution of the lifetime spectra of the samples FAY1 and NAHf.

(a) Properties of the α-Al_2O_3 surfaces. In both samples we found that for low positron injection energies E_{e^+}
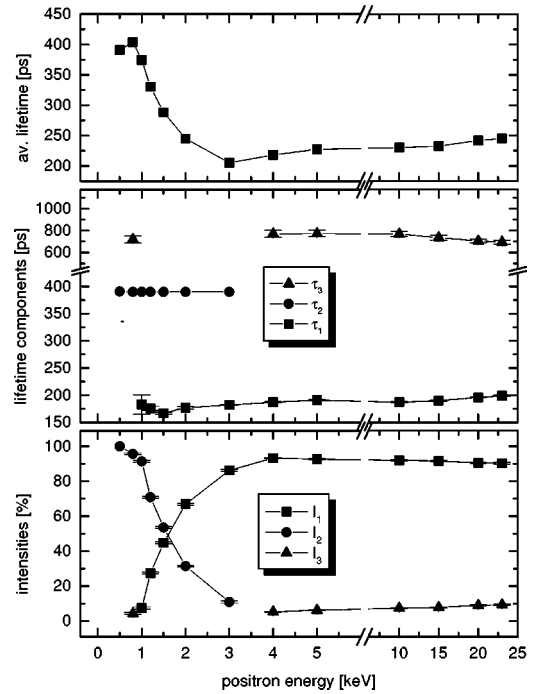
$= 0$–0.5 keV the spectra consisted of single lifetime components, $^{(FAY1)}\tau = 368$ ps and $^{(NAHf)}\tau = 391$ ps. For higher injection energies, the long lifetime components were still resolved from the spectra, but their intensities became smaller with increasing positron injection energy. We therefore ascribe this component to positrons diffusing back to the surface, where they are trapped and annihilated in the long-lifetime sites. The value of this surface lifetime is smaller than that found by Brauer *et al.* in sieve granulated and spray-dried granulated Al_2O_3 powders after sintering, $\tau_2 = 400$–480 ps.[33]

The slight differences in the lifetimes of these surface components indicate a small difference in the surface state for the positrons. This is possibly due to differences in the types of impurities segregated at the surface. The presence of impurities probably also causes the surface states to have positron lifetimes smaller than those reported by Brauer *et al.* Comparing these values with those obtained from the amorphous films, cf. Figs. 12 and 13, the annihilation rate at the surfaces of the films grown by substrate oxidation is lower.

(b) Properties of the bulk films. For convenient comparison of the major lifetime in both oxidation grown films, τ_1 in Figs. 8 and 9, we have put them together in Fig. 10.

α-Al_2O_3 on NAHf. For a 400 nm thick film, as stated in Sec. III B 1, and assuming the positron implantation to follow a Makhov profile with the parameters given in Sec. II E, one calculates the fraction of positrons implanted in the substrate to be $\approx 1\%$, for a positron injection energy of 5 keV. Very few positrons will back diffuse from the substrate to the metal-oxide interface. Also, taking into account the number of positrons that will forward-diffuse from the oxide film to
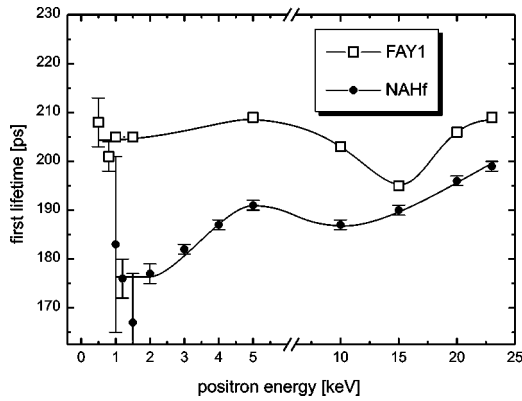
FIG. 10. Major lifetime component, τ_1, in the samples NAHf and FAY1, cf. Table I.

the interface, one calculates that not more than 2% of the injected positrons can be trapped and annihilated at this interface. Therefore, the increase in the average positron lifetime from 205 to 227 ps, see plot in Fig. 9, for positron injection energies ranging from 3–5 keV, must be entirely due to structural changes in the Al_2O_3 layer. The first lifetime component, τ_1, changes from 182 to 191 ps in this range, see Fig. 10. The latter value is in good agreement with the analysis of the CONTIN program:[52,53] $^{(NAHf)}\tau_1(5 \text{ keV})$ $= 194$ ps.[17] All these values are higher than that given by Forster *et al.*[54] or Schaefer and Forster[55] for single vacancies in an Al_2O_3 (sapphire) single crystal: $\tau_{1v} = (160 \pm 20)$ ps.

Because the value of τ_1 changes from 177 ps at 1–2 keV to 191 ps at 5 keV, we consider this component to be a mixture of signals from different multiple vacancies. According to the change of the lifetime value the size of these small vacancy clusters should increase from the outer surface to the interface. Schaefer and Forster found in an electron-irradiated Al_2O_3 single crystal (sapphire) the known aggregation and annealing out of oxygen vacancies at about 600 K not to be reflected in the positron lifetime data, and conclude that either the density of aluminum vacancies exceeds the density of oxygen vacancies by far or that the oxygen vacancies do not trap positrons due to positive charge.[55] If we follow the hypothesis that oxygen vacancies are not detectable by positron spectroscopy, our results are not consistent with what we expect from the diffusion model of layer growth. Then, the inner part should exhibit a smaller deficit of aluminum than the surface of the layer, and, hence, the vacancy clusters should be smaller at the interface.

We find, however, the behavior that the size of the trapping sites seems to increase with the depth. Atobe *et al.* report in neutron irradiated Al_2O_3 the existence of electron-doped oxygen vacancies and oxygen double vacancies, F and F_2 centers, by their optical activity.[56] These should be able to act as positron traps as long as they do not lose electrons and become positively charged F^+ or F_2^+ centers.

It is very likely that in our samples oxygen vacancies or double vacancies can act as positron traps, as the layer grows by diffusion of oxygen vacancies. Atobe *et al.* demonstrated that all neutron induced defects are annealed out at temperatures of 800 °C or higher, but we think this does not negate the possibility of our specimens having frozen-in oxygen va-

cancies, because they were rapidly cooled from their high-temperature oxidation conditions, and are not at conditions of thermodynamic equilibrium. While the oxide layers were growing at high temperature, at diffusion-controlled rates, there was always a deficiency of oxygen atoms at the oxide/substrate interface, and a deficiency of aluminum atoms at the surface, giving rise to a likely formation of multivacancies of oxygen at the interface. Therefore, the increase of the first lifetime component as a function of positron injection energy might be attributed to a transition from aluminum multiple vacancies to oxygen multiple vacancies as major positron traps. Also, this might be the reason for the increase of the S parameter as described in Sec. III B 1. Another support for this hypothesis may be the decrease of the density of nickel impurities with respect to depth. Nickel impurities may act as traps for oxygen vacancies according to the reaction

$$2 \text{ NiO} \xrightarrow{Al_2O_3} 2 \ [Ni_{Al}]^{--} + 2 \ [O_O] + [V_O]^{++}. \quad (6)$$
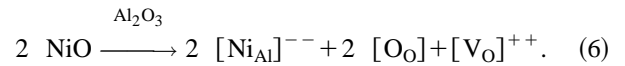
Besides the surface component, we found no indication for vacancy clusters of intermediate size inside the layer exhibiting positron lifetimes of 300–400 ps as reported by Schaefer and Forster.[55] We ascribe this also to the nonequilibrium state of our samples, where larger voids act as effective drains for aluminum or oxygen atoms or as a source for their respective vacancies and, hence, are not stable.

α-Al₂O₃ on FAY1. Contradictory to the changes in the first lifetime component in NAHf, the one associated with FAY1 exhibits a rather constant value over a wide range of positron implantation energy, $E_{e^+} = 0.5–10$ keV. Together with the constant value of the average positron lifetime, cf. Fig. 8, it indicates that the defects in the film are uniformly distributed across the depth. The average value of the first component in that region was found to be $\tau_1 = 205$ ps, in very good agreement with the calculations of the CONTIN program: $^{(FAY1)}\tau_1(5 \text{ keV}) = 206$ ps.[17] This value is markedly larger than that for the film on sample NAHf.

No information about positron lifetimes in multiple-vacancy defects in α-Al_2O_3 is presently available. It cannot be determined from our data whether the increased defect lifetime in the FAY1 film is due to larger vacancy clusters or to a different electronic structure of the trapping site, effected by a different chemical environment. Possibly, the film on the NAHf specimen contains more impurities that can be attached to the trapping sites, and these contribute electrons that annihilate the positrons more rapidly, causing their lifetimes to be shorter.

The drop of the first lifetime component to a value of $\tau_1 = 195$ ps at 15 keV positron implantation energy, also shown in the average positron lifetime in Fig. 8, corresponds to the rise of the S parameter at this energy, cf. Fig. 2. It is attributed to a change in the defect structure of the film in the vicinity of the oxide-substrate interface, perhaps due to increased impurity density, or due to a rough interface layer.

(c) Properties of the substrates. If we assume that the positron implantation follows a Makhov profile,[21,22] and we consider in the case of FAY1 the thickness of the alumina

layer on the Fe$_3$Al substrate to be 1.7 μm approximately, cf. Sec. III B 1, we conclude that for positron injection energies of $\leq$10, 15, 20, and 23 keV approximately 0, 3.5, 25, and 42 % of all positrons, respectively, can reach the iron aluminide substrate; for the nickel aluminide substrate the respective values are 49, 82, 93, and 95 %.

Here we assume that the positrons are trapped in the vicinity of their thermalization points, which is reasonable, because the lifetime values clearly indicate saturated trapping. Correcting for the lifetime components due to annihilation in the overlying oxide film, we estimate that the spectrum of the FAY1 substrate consists of two lifetime components of 220 and 650 ps, approximately. We can be certain that the first lifetime component is higher than 200 ps and, hence, originates from small vacancy clusters instead of monovacancies in the unoxidized substrate. Comparing this with the spectrum obtained from the unoxidized substrate, cf. Sec. III A, it is seen that the defect structure of the substrate is changed in the interface region during the oxidation process. Under high-temperature oxidation conditions, the films and substrate were not in thermodynamical equilibrium due to the ongoing oxidation process, and defects due to oxidation were frozen in when they were cooled. Positron traps in the substrate of the oxidized samples are quite different from those of the unoxidized stage, cf. Sec. III A. Here, small vacancy clusters and larger voids are the major positron traps in the substrate in the immediate vicinity (1–2 μm) of the substrate-oxide interface.

If we assume the first lifetime component to originate from double vacancies, having a positron trapping coefficient of $\mu_{nv} = n\mu_{1v} = 2 \times 10^{15}$ s^{-1} and diffusion constant of $D_+ = 1$ cm^2/s similar to other metals like iron, cf. Vehanen et al.,[57] and copper, cf. Schaefer et al.,[58] or aluminum, cf. Mills and Wilson ($^{(Al)}D_+ = (0.76 \pm 0.14)$ cm^2/s),[59] and using the calculated positron diffusion length of $^{(FAY1)}L_+^{(s)} \approx 40$–60 nm, cf. Fig. 15, one calculates, applying formula (A4), see the appendix, the density of the double vacancies to be $c_{2v} \approx 100$–240 ppm.

The spectrum taken at a positron energy of 23 keV in the NAHf sample consists, as already mentioned above, almost entirely of annihilation events originating from the substrate. Thus, the substrate in the vicinity of the interface is believed to exhibit a lifetime spectrum with $\tau_1 \approx 200$ ps, $I_1 \approx 90\%$ and $\tau_2 \approx 650$ ps, $I_2 \approx 10\%$, that is caused by positrons trapped in double vacancies and much larger vacancy clusters. We make this conclusion from the analogy of the defect free materials of iron or nickel, having lifetimes of $^{(Fe)}\tau_b = 104$ ps (Ref. 57) and $^{(Ni)}\tau_b = 104$ ps,[60] respectively, and their respective mono and double vacancy lifetimes of $^{(Fe)}\tau_{1v} = 175$ ps,[57] $^{(Ni)}\tau_{1v} = 142$ ps,[61] $^{(Fe)}\tau_{2v} \approx 200$ ps,[62] and $^{(Ni)}\tau_{2v} = 220$ ps.[60] The change from the unoxidized sample, cf. Sec. III A, is rather large. The loss of aluminum in the vicinity of the interface and the associated diffusion controlled transport of aluminum atoms to that interface from the bulk substrate creates vacancies that perhaps partially aggregate.

According to the estimations mentioned above, we conclude that the spectra taken from the sample NAHf at posi-

TABLE II. Comparison of the positron lifetime parameters in iron and nickel aluminides before and after thermal oxidation, cf. Table I; lifetimes are given in picoseconds (ps), intensity of the component in parentheses.

	Ni$_{49}$Al$_{51}$Hf$_{0.05}$	Fe$_{69.9}$Al$_{28}$Cr$_2$Y$_{0.1}$
As cast	$\tau_1 = 172 \pm 1$	$\tau_1 = 165 \pm 1$
		$\tau_2 = 291 \pm 3$ (27%)
Oxidized	$\tau_1 \approx 200$	$\tau_1 \approx 220$
	$\tau_2 \approx 650$ (10%)	$\tau_2 \approx 650$ (10%)

tron energies of 20 and 23 keV originate from the substrate only. Comparing these points in Fig. 7 with the single component lifetime spectrum obtained from the unoxidized sample, cf. Sec. III A, the defect structure of the substrate specimen is obviously changed in the vicinity of the interface, cf. Table II.

C. Film formed by plasma deposition

1. Doppler-broadening results

Figure 11 shows that the S-parameter profile for the aluminum oxide film grown by plasma deposition, is completely different from those of the films grown on the iron and nickel aluminide substrates by oxidation, cf. Figs. 2, 3, 6, and 7. The S parameter of this film is markedly higher than in the thermally grown oxides and even higher than at the surface. This is attributed to open-volume traps of larger size, which is a reasonable assumption, since the film is amorphous, as well as to a chemical environment different from those of the oxidation-grown films.

According to the film-producing procedures, cf. Table I, this layer should be free of impurities originating from the substrate, whereas the thermally grown films contain non-negligible densities of their respective transition-metal at-
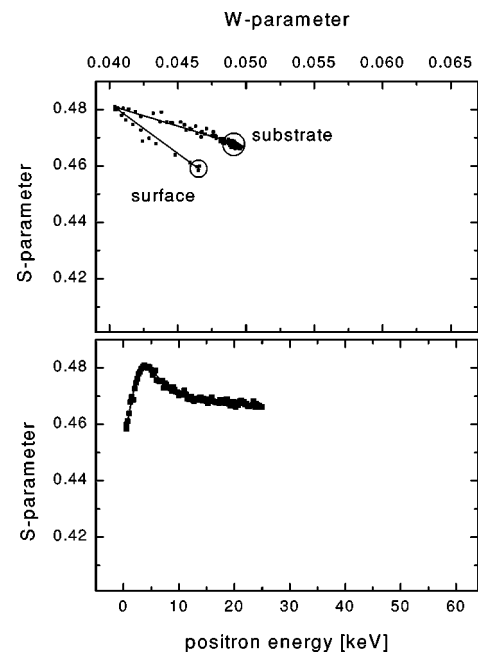
FIG. 11. S parameter in sample NA as a function of positron energy and S vs W plot.

oms. It is known that the probability of high-momentum electron annihilation is much larger in nickel than in aluminum, which causes a decrease in the S parameter, see for example, Asoka-Kumar *et al.*[63] The iron will have the same effect. We, therefore, conclude that the impurities in the oxidation-grown films will somewhat lower the S parameter. Nevertheless, this should not be enough to explain this dramatic increase in the S-parameter value, cf. Sec. III B 1, if we consider the results of Vehanen *et al.*[23] They report in impurity-free α-Al_2O_3 a decreasing S parameter from the surface to the bulk. We, hence, assume that the different, noncrystalline structure causes the positrons to annihilate mostly with low-momentum electrons in the amorphous Al_2O_3 film on sample NA.

The data points in the S vs W plot spread along two lines and cluster at (W, S) pairs for the three different stages surface, film, and substrate. This indicates a uniform Al_2O_3 film with no preferred trapping at the substrate film interface, as was expected from the film generation procedure.

The thickness of the film on the NA substrate was reported to us as about 1 μm, but this is in question. Assuming that thickness, we were totally unable to obtain even a poor quality fit to the data with VEPFIT calculations. From the S-parameter curve we do not get any indication for a structure in the layer or preferred trapping at the interface. The smooth S-parameter curve is in agreement with the expectations from the way the Al_2O_3 film was generated, cf. Table I, which should produce a uniform film. Even if the density of the Al_2O_3 layer was chosen unreliably low at 2 g/cm^3, the fitted layer thickness was as low as 460 nm. Therefore, we assume the layer to be much thinner than presumed. The range 3.5 $g/cm^3 < {}^{(Al_2O_3)}\rho_l < 3.97$ g/cm^3 in which the real density should fit gives the thickness values (193 ± 23) nm $> d_l > (156 \pm 22)$ nm. From those VEPFIT calculations we obtain the positron diffusion length in layer, $L_+^{(l)}$, and substrate, $L_+^{(s)}$, to be $L_+^{(l)} = 24 \ldots 29 (\pm 1)$ nm and $L_+^{(s)} = 88 \ldots 84 (\pm 20)$ nm, respectively for the lowest and highest density.

2. Results of variable energy positron lifetime spectroscopy

The rather slow drop of the surface component, cf. Fig. 12, indicates a much longer positron diffusion length, that we did not expect from the S-parameter measurements in Sec. III C 1. Here, any second component, besides the surface component, starts not earlier than at an energy of 2 keV, at which the surface component in the α-Al_2O_3 layers is dropped to 30% (NAHf) or already disappeared (FAY1).

The first appearance of the main component in the film is at 4 keV positron energy. That means the trapping coefficient for this component is markedly smaller than for the other components, as its intensity goes up to 86% deeper in the layer. Therefore, the trapping into this defect is obviously not *diffusion limited* but *transition limited*,[64,65] which is usually assumed for small vacancy clusters having that lifetime value. As we know from the micrographs, the outer surface of the layer is quite smooth, not structured as the α-Al_2O_3 films.[14] The positrons, hence, really have to diffuse back to the surface.

If we use Eq. (4) and take the disappearance of the surface component as the value for determining the positron diffu-
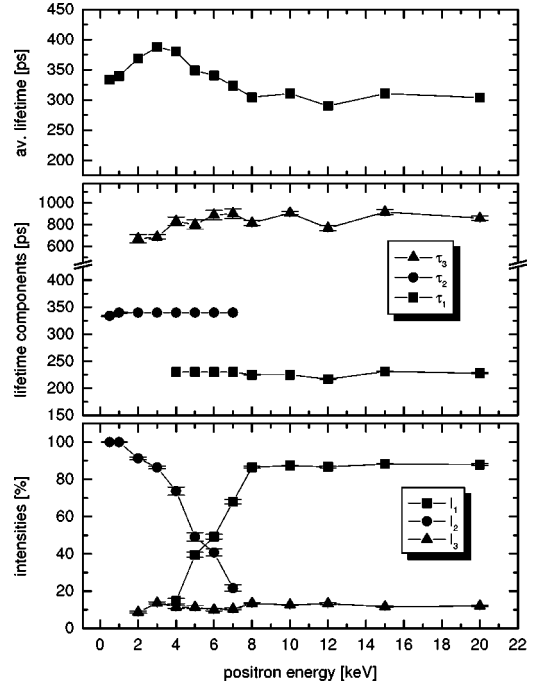
FIG. 12. Positron lifetime parameters as a function of energy in sample NA, cf. Table I. If no error bars are drawn, error bars are smaller than the symbol size; lines are to guide the eye.

sion length we calculate ${}^{(NA)}L_+^{(l)} = 115$ nm. That is much higher than the value of $L_+^{(l)}$ calculated from the S-parameter curve in Sec. III C 1, $L_+^{(l)} \approx 30$ nm.

Obviously, the positron traps in the amorphous layer are different from the α-Al_2O_3 layers. The main component exhibits a lifetime value of $\tau_1 = 225 - 230$ ps which is much higher than in the oxidation-grown films, cf. Sec. III B 2. The positron lifetime in a vacancy cluster in crystalline materials as a function of aggregated single vacancies follows a function that has a square-root shape, as long as few single vacancies are clustered.[62] Assuming the positron lifetime in amorphous materials exhibits a similar behavior, we conclude that the diameter of the open volume acting as the origin for this lifetime component is roughly 2–3 atomic distances.

Considering the positron diffusion length to be 30–40 nm in the plasma deposited film, there is no evidence for preferred trapping of positrons at the interface substrate layer. Hence, we assume the interface to be almost defect free in agreement with the Doppler-broadening results in Sec. III C 1.

In the same way as described in Sec. III B 2 we calculate with the layer thickness of $d_l = 185$ nm, cf. Sec. III C 1, that at the positron energies of 15 and 20 keV, 96 and 98 % of all positrons are implanted in the substrate. Comparing the results we obtained from the raw substrates, see Sec. III A, where we found annihilation in monovacancies, the defect structure of the substrate is changed by the plasma deposition, at least in the measurable vicinity of the interface. Here we find annihilation in small vacancy clusters of few aggregated vacancies ($n \approx 4$) and larger clusters. This is likely the result of the first impact during the plasma deposition procedure, which is almost like ion implantation and can, therefore, create vacancylike defects.[66]
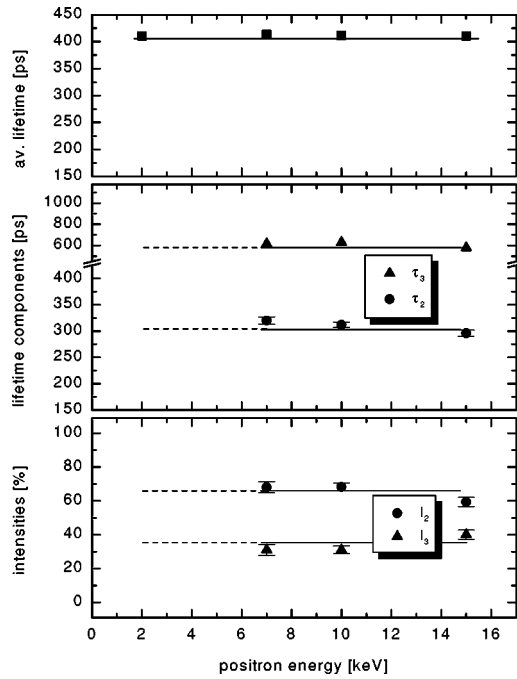
FIG. 13. Positron lifetime parameters as a function of energy in sample FAZr, cf. Table I. If no error bar is shown the error is smaller than the symbol size; lines are to guide the eye. The indices have been chosen to fit in with the components in Figs. 8, 9, and 12.

FIG. 14. S parameter in sample FAZr as a function of positron energy and S vs W plot.

Applying formula (A4), cf. the Appendix, and using $L_+^{(s)} \approx 85$ nm, see Sec. III C 1, and $\mu_{4v} = 4 \times 10^{15}$ s^{-1} as mentioned above and in Sec. III B 2, one calculates the cluster density to be in the range $c_{4v} \approx 10$–20 ppm.

D. Film formed by physical vapor deposition

Both the positron lifetime measurements and the Doppler broadening results indicate that the composition and structure of this film varies very little with respect to depth. Figure 13 shows plots, as a function of positron injection energy, of the average positron lifetime, and of the two individual lifetime components that were deconvoluted from the spectra. The average positron lifetime does not change with injection energy. For injection energies of 7 keV or greater the two lifetime components do not change very much in either magnitude or intensity.

The spectrum obtained at 2 keV positron injection energy was somewhat disturbed by a satellite peak appearing 6.37 ns after the main peak, causing an unstable decomposition. In spite of this, the average positron lifetime of the different spectra decompositions was always the same as shown in Fig. 13. We, therefore, assume the proper decomposition to be the same as resulting from the other spectra. This is consistent with the results of the Doppler broadening measurement, cf. Fig. 14.

It is surprising that no surface component was separable from a bulk or defect component in sample FAZr, see Fig. 13. The change in the average lifetime $\bar{\tau}$ during the run was negligible compared to the other films. We believe that it is reasonable to ascribe the component having lifetime values of $\tau_2 = 300$–320 ps to surface trapping because its value is close to that of the other amorphous film, cf. Fig. 12, and,

therefore, to conclude that the implanted positrons annihilate from very similar states: Inside the physical vapor deposited film, the positrons are trapped at the same centers as at the physical surface, which implies larger voids in the layer on their internal surfaces the positrons are trapped. This idea is also suggested by the fact that the S parameter does not change at all from the surface to the interior of the film, cf. Fig. 14, even in the very first energy steps of 0.5 and 1 keV. The intensity of the long lifetime component, I_3, is three times as high as in the other layers. That also indicates the presence of more large voids inside the layer.

If we compare the surface S parameter of the film on FAZr with that on NA, we find both values exactly the same, cf. Figs. 11 and 14. That supports the assumption that, inside the physical vapor deposited film, the same open volume configurations act as positrons traps as at the outer surface of both amorphous layers, even though the W parameter is slightly different.

As the layer is 5 μm thick, one calculates using the parameters given in Sec. II E that at a positron energy of 30 keV 17% and at an energy of 40 keV 32% of all positrons are implanted in the substrate. Therefore, the very slight decrease of the S parameter as well as the slight increase of the W parameter at positron energies above 30 keV, cf. Fig. 14, can be attributed to positrons implanted into the substrate.

IV. SUMMARY

All of the α-Al$_2$O$_3$ layers examined in this study exhibited very similar S-parameter values, see Fig. 15, independent of the substrate. Taking into account the similar positron lifetime results on NAHf and FAYI we conclude that the defect structure of all outer parts of oxidation-grown films was basically the same. It consists of a single kind of
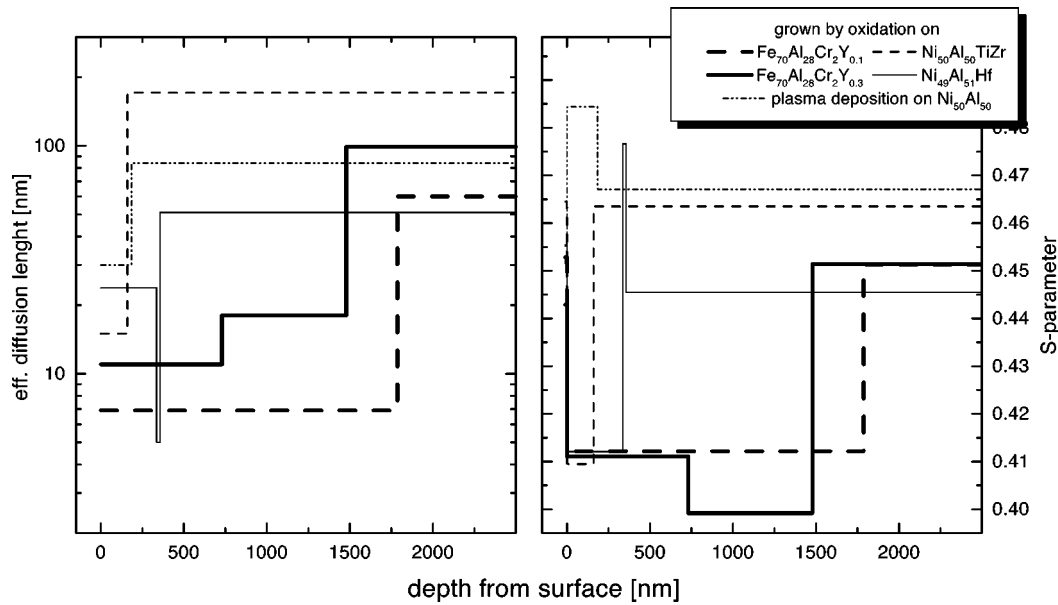
FIG. 15. Positron diffusion lengths and S parameters as a function of depth as calculated by VEPFIT. The absolute S-parameter values of samples FAY1 and NAHf, cf. Table I, are adjusted for comparison by using formula (5).

small vacancy clusters in the range of 2–4 aggregated mono-vacancies, most likely divacancies, and much larger vacancy clusters as well. Owing to the small positron diffusion lengths, which were consistent despite several methods of calculation, cf. Table III, those clusters must be uniformly located in the matrix and not just at grain boundaries.

Slight differences were noted between the different substrates. The slightly higher positron diffusion length in the alumina films on the nickel aluminide substrates indicated that the density of vacancy clusters in these films is slightly lower than those grown on iron aluminide substrates. Based on the positron lifetime parameters with respect to depth, the films on nickel aluminide substrates appeared to show an increase in the defect size with depth. This may be related to the parabolic growth rate where the film grows more slowly at longer times, allowing larger vacancy clusters to form. In contrast, the films on iron aluminides had a uniform positron lifetime parameter, indicating a rather uniform defect structure with respect to depth, but nonuniform by its S and W parameters. This may be a result of the two-layered grain structure observed on these substrates compared to the more uniform alumina layers grown on nickel aluminides. With an increase in the amount of Y in the iron aluminide substrate, there appeared to be a finer inner-layer grain size. This was

TABLE III. Comparison of the positron diffusion lengths, $L_+^{(l)}$ (nm), in the Al_2O_3 films on the samples in Table I, calculated by different methods; DBAR indicates S-parameter measurements, POLIS indicates positron lifetime spectroscopy.

Sample	FAY1	FAY3	NATZ	NAHf	NA
Eq. (4)					
DBAR	17	16	19	19	6.8
VEPFIT	9	11	15	24	30
Eq . (4)					
POLIS	8			22	100

attributed to larger amounts of Y resulting in a larger inhibition in grain growth in the alumina film.

In general, the reasons for these slight differences in the alumina layers grown on the two types of aluminide substrates has not been conclusively identified but may be related to differences between Ni versus Fe incorporation in the films. An additional variable is the method by which the dopant additions were added (alloy additions of Hf and Zr in nickel aluminides and yttrium oxide additions to iron aluminides). Further work will be required to isolate these effects.

Positron lifetime results show that the defect structures of the substrates were drastically changed during the oxidation process, leaving a high density of double vacancies, c_{2v} = 100–200 ppm, and, in FAY1, larger voids in the range of at least a few microns next to the interface. These larger voids are of the correct size range to cause early spallation as has been noted on longer times to form larger voids in the substrate or at the oxide-substrate interface which contribute to spallation of the alumina layer. Future work will concentrate on changes in the defect structure of the substrates with increasing oxidation time.

For the deposited amorphous alumina film, a higher positron lifetime was observed, indicating larger vacancy clusters compared to crystalline α-Al_2O_3. However, a dramatically different S and W parameter gave evidence of a totally different electronic structure of the trapping site. Also, the creation of 10–20 ppm of small vacancy clusters in the substrate likely reflects the high energy (similar to ion implantation) used in the early stages of this deposition method. For the vapor-deposited film, no difference was noted between the surface and the interior of the film, indicating a high density of large cavities that act as internal surfaces, which was not observed in the other types of films.

These results for alumina films indicate that positron spectroscopy can be used to:

(i) Characterize defect types and their distributions in Al_2O_3 films/scales.

(ii) Examine the influence of presence of dopants in the alumina scales on the defect environment.

(iii) Determine changes in substrate defect distribution due to transport processes associated with oxide growth.

APPENDIX

As already published elsewhere,[48] it is possible to estimate the minimum values of the densities of two defects, $c_i = \kappa_i / \mu_i$, $i = 1,2$, κ is the trapping rate, μ is the trapping coefficient, even if saturated trapping, $I_1 + I_2 = 1$, occurs. In this case the ratio

$$\frac{\kappa_1}{\kappa_2} = \frac{I_1}{I_2} \tag{A1}$$

applies. Considering the relation

$$\tau_{\text{eff}} = \frac{1}{\lambda_b + \kappa_1 + \kappa_2} \tag{A2}$$

from the trapping model of two noninteracting defects, where λ_b is the positron annihilation rate in the defect free bulk and κ_1 and κ_2 are the trapping rates for the two defects, respectively, one derives from

$$L_+ = \sqrt{6 D_+ \tau_{\text{eff}}}, \tag{A3}$$

the equation to calculate the positron diffusion length,[64] with the estimation $I_1 + I_2 \approx 1$ and using Eq. (A1),

$$c_1 = \frac{I_1}{I_2 \mu_1} \left[\frac{6 D_+}{L_+^2} - \lambda_b \right], \quad c_2 = \frac{I_2}{I_1 \mu_2} \left[\frac{6 D_+}{L_+^2} - \lambda_b \right] \tag{A4}$$

as the values for the defect densities.

*Author to whom correspondence should be addressed. Electronic address: somieskib@ornl.gov

[1] *Proceedings of the International Symposium on Nickel and Iron Aluminides: Processing, Properties, and Applications,* edited by S. C. Deevi, V. K. Sikka, P. J. Maziasz, and R. Cahn (American Society for Metals, Materials Park, Ohio, 1997).

[2] B. A. Pint, Oxid. Met. **45**, 1 (1996).

[3] P. Kofstad, *High Temperature Corrosion* (Elsevier Applied Science, London, 1988).

[4] H.-E. Schaefer, Phys. Status Solidi A **102**, 47 (1987).

[5] P. Hautojärvi, Mater. Sci. Forum **175-178**, 47 (1995).

[6] T. Hyodo, in *Positron Annihilation*, edited by P. C. Jain, R. M. Singru, and K. P. Gopinathan (World Scientific, Singapore, 1985), pp. 643–656.

[7] B. A. Pint, P. F. Tortorelli, and I. G. Wright, Mater. Corros. **47**, 663 (1996).

[8] B. A. Pint, Mater. Sci. Forum **251-254**, 397 (1997).

[9] I. G. Brown and Z. Wang, in *9th Annual Conference on Fossil Energy Materials* (U.S. Dept. of Energy, Conf-9505204, ORNL/FMP-95/1, Oak Ridge, TN, 1995), p. 239.

[10] O. R. Monteiro, Z. Wang, and I. G. Brown, J. Mater. Res. **12**, 2401 (1997).

[11] O. R. Monteiro, Z. Wang, P. Y. Hou, and I. G. Brown, Nucl. Instrum. Methods Phys. Res. B **127-128**, 821 (1997).

[12] T. W. Barbee (private communication).

[13] B. A. Pint, Oxid. Met. **48**, 303 (1997).

[14] B. A. Pint, K. B. Alexander, and E. Dickey (unpublished).

[15] K. G. Lynn and H. Lutz, Rev. Sci. Instrum. **51**, 977 (1980).

[16] R. Suzuki *et al.*, in *Slow Positron Beam Techniques for Solids and Surfaces*, AIP Conf. Proc. No. 303, edited by E. Ottewitte and A. H. Weiss (AIP, New York, 1994), p. 526.

[17] J. Xu *et al.*, Appl. Phys. Lett. **71**, 3165 (1997).

[18] T. E. M. Staab, B. Somieski, and R. Krause-Rehberg, Nucl. Instrum. Methods Phys. Res. A **381**, 141 (1996).

[19] H. Schut and A. van Veen, Appl. Surf. Sci. **85**, 225 (1995).

[20] A. van Veen *et al.*, Appl. Surf. Sci. **85**, 216 (1995).

[21] S. Valkealahti and R. M. Nieminen, Appl. Phys. A: Solids Surf. **32**, 95 (1983).

[22] S. Valkealahti and R. M. Nieminen, Appl. Phys. A: Solids Surf. **35**, 51 (1984).

[23] A. Vehanen, K. Saarinen, P. Hautojärvi, and H. Huomo, Phys. Rev. B **35**, 4606 (1987).

[24] M. J. Puska, program LIFESPECFIT, Teknillinen Korkeakoulu, Otaniemi (Finland), 1978.

[25] R. N. West, in *Positrons in Solids*, edited by P. Hautojärvi, Topics in Current Physics, Vol. 12 (Springer, Berlin, 1979), pp. 89–144.

[26] M. Clement, J. M. M. de Nijs, P. Balk, H. Schut, and A. van Veen, J. Appl. Phys. **81**, 1943 (1997).

[27] M. Clement, J. M. M. de Nijs, P. Balk, H. Schut, and A. van Veen, J. Appl. Phys. **79**, 9029 (1996).

[28] M. Hasegawa, Y. Nagashima, K. Kawashima, T. Hyodo, S. Yamaguchi, M. Forster, and H.-E. Schafer, Nucl. Instrum. Methods Phys. Res. B **91**, 263 (1994).

[29] Y. Nagashima, K. Kawashima, T. Hyodo, M. Hasegawa, K. Hirage, S. Yamaguchi, M. Forster, and H.-E. Schaefer, Mater. Sci. Forum **175-178**, 461 (1995).

[30] T. v. Hoecke, D. Segers, H. Schut, C. Dauwe, A. van Veen, B. van Waeyenberge, and L. Palffy, Mater. Sci. Forum **255-257**, 724 (1997).

[31] C. Dauwe and Mbungu-Tsumbu, Phys. Rev. B **45**, 9 (1992).

[32] F. Ewertowski, T. Majcherczyk, B. Rozenfeld, and A. Baranowski, J. Phys. Chem. Solids **44**, 609 (1983).

[33] G. Brauer, F. Kerbe, Z. Kajcsos, and A. Ashry, Phys. Status Solidi A **84**, 451 (1984).

[34] P. Asoka-Kumar (private communication).

[35] Y. Jirásková, O. Schneeweiß, M. Šob, I. Novotný, I. Prochazka, F. Bečvář, B. Sedlák, F. Šebesta, and M. J. Poska, J. Phys. IV **5**, C1-157 (1995).

[36] H.-E. Schaefer, R. Würschum, M. Šob, T. Žák, W. Z. Yu, W. Eckert, and F. Banhard, Phys. Rev. B **41**, 11 869 (1990).

[37] J. C. Wang, D. J. Liu, M. X. Chen, and X. X. Cai, Scr. Metall. Mater. **25**, 2581 (1991).

[38] G. Dlubek, O. Brümmer, J. Yli-Kauppila, and J. Johansson, Phys. Status Solidi B **106**, K83 (1981).

[39] B. Bergersen and M. J. Stott, Solid State Commun. **7**, 1203 (1969).

[40] A. Seeger, Appl. Phys. **4**, 183 (1974).

[41] C. G. Hübner, T. E. M. Staab, and R. Krause-Rehberg, Appl. Phys. A: Solids Surf. **61**, 203 (1995).

[42] M. Shimotomai, T. Iwata, and M. Doyama, Philos. Mag. A **51**, L49 (1985).

[43] M. Shimotomai, T. M. Wang, and M. Doyama, J. Nucl. Mater. **116**, 347 (1983).

[44] S. M. Kim, Mater. Sci. Forum **15-18**, 1323 (1987).

[45] C. L. Fu, Y.-Y. Ye, M. H. Yoo, and K. M. Ho, Phys. Rev. B **48**, 6712 (1993).

[46] W. Deng, L. Xiong, C. Lung, S. Wang, and J. Guo, Mater. Sci. Forum **175-178**, 339 (1995).

[47] Y.-K. Park and J. T. Waber, Scr. Metall. **19**, 1095 (1985).

[48] B. Somieski and R. Krause-Rehberg (unpublished).

[49] K. Saarinen, P. Hautojärvi, A. Vehanen, R. Krause, and G. Dlubek, Phys. Rev. B **39**, 5287 (1989).

[50] J. Fang, A. M. Thompson, M. P. Harmer, and H. M. Chan, J. Am. Ceram. Soc. **80**, 2005 (1997).

[51] B. Somieski and B. A. Pint (unpublished).

[52] R. B. Gregory and Y. Zhu, Nucl. Instrum. Methods Phys. Res. A **290**, 213 (1990).

[53] R. B. Gregory and Y. Zhu, Nucl. Instrum. Methods Phys. Res. A **302**, 496 (1991).

[54] M. Forster, J. Mundy, and H.-E. Schaefer, in *Positron Annihilation*, edited by L. Dorikens-Vanpraet, M. Dorikens, and D. Seg-ers (World Scientific, Singapore, 1988), pp. 833–836.

[55] H.-E. Schaefer and M. Forster, Mater. Sci. Eng., A **109**, 161 (1989).

[56] K. Atobe, N. Nishimoto, and M. Nakagawa, Phys. Status Solidi A **89**, 155 (1985).

[57] A. Vehanen, P. Hautojärvi, J. Johansson, J. Yli-Kauppila, and P. Moser, Phys. Rev. B **25**, 762 (1982).

[58] H.-E. Schaefer, W. Stuck, F. Banhart, and W. Bauer, Mater. Sci. Forum **15-18**, 117 (1987).

[59] A. P. Mills and R. J. Wilson, Phys. Rev. A **26**, 490 (1982).

[60] N. Meyendorf, R. Krause-Rehberg, B. Somieski, R. Kern, and I. Altpeter, Technical Report No. 960223-TW, Fraunhofer Institute for NDT, Saarbrücken, Germany (unpublished).

[61] K. G. Lynn, C. L. Snead, and J. J. Hurst, J. Phys. F **10**, 1753 (1980).

[62] M. J. Puska, Phys. Status Solidi A **102**, 11 (1987).

[63] P. Asoka-Kumar, M. Alatato, V. J. Ghosh, A. C. Krauseman, B. Nielsen, and K. G. Lynn, Phys. Rev. Lett. **77**, 2097 (1996).

[64] R. M. Nieminen and M. J. Manninen, in *Positrons in Solids* (Ref. 25), pp. 145–195.

[65] K. Peterson, in *Positron Solid-State Physics*, edited by W. Brandt and A. Duspaquier (North-Holland, Amsterdam, 1983), pp. 298–358.

[66] I. Brown, A. Anders, S. Anders, M. R. Dickinson, R. MacGill, O. R. Monteiro, E. M. Oks, S. Raoux, Z. Wang, and G. Yoshkov, in *Ion-Solid Interaction for Materials Modification and Processing*, edited by D. B. Poker *et al.,* MRS Symposia Proceedings No. 396 (Materials Research Society, Pittsburgh, 1996), p. 467.